JMM

Lump wave dynamics and interaction analysis for an extended (2+1)-dimensional Kadomtsev-Petviashvili equation

Majid Madadi[†*], Esmaeel Asad[†,‡]

[†]*Department of Mathematics, Institute for Advanced Studies in Basic Sciences (IASBS),*
P.O. Box 45137-66731, Zanjan, Iran
[‡]*School of Mathematics, Institute for Research in Fundamental Sciences (IPM), P.O. Box 19395-5746,*
Tehran, Iran
Email(s): mmadadi@iasbs.ac.ir, easadi@iasbs.ac.ir

Abstract. Constructing exact solutions for high-dimensional nonlinear evolution equations and exploring their dynamics are critical challenges with significant practical implications. The extended Kadomtsev-Petviashvili (eKP) equation, a key example of an integrable two-dimensional equation, highlights the importance of these studies. A logical extension is to investigate lump wave solutions in this context. In this paper, we introduce novel constrained conditions into $N-$soliton solutions for a $(2+1)$-dimensional eKP equation. We present a theorem to analyze the asymptotic behavior of the N-soliton solution. This analysis leads to the derivation of lump waves, along with the determination of their trajectories and velocities. To investigate the interaction between higher-order lumps and soliton waves, as well as breather waves, we employ the long wave limit method. We analyze the trajectory equations governing the motion before and after the collision of lumps and other waves and identify conditions under which the lump wave avoids collision with other waves. Several figures are included to illustrate the physical behavior of these solutions.

Keywords: Hirota bilinear, soliton solution, lump wave, breather wave.
AMS Subject Classification 2010: 37K40, 70Kxx.

1 Introduction

The Hirota bilinear method [6] is a powerful technique for solving nonlinear evolution equations. It has gained popularity among scholars due to its directness and simplicity in constructing multiple soliton solutions for nonlinear partial differential equations [9, 16, 19].

Lump waves, which are rational function waves localized in all directions in space and time, have attracted significant attention. Various methods such as inverse scattering transformation [11], Grammian determinant method [14], Darboux transformation [18], and the long wave limit method [1] have been developed to study lump waves.

One direct method for obtaining soliton, breather, and lump wave solutions is the widely used "Ansatz" technique [10, 17]. An ansatz is essentially an educated guess or assumed form for the solution of a problem. This form typically involves unknown parameters or functions, which are later determined by substituting the ansatz into the original equation and solving the resulting conditions. In contrast, the long wave limit method [12] offers a more systematic approach for deriving lump wave solutions. By reducing wave numbers to zero, it transforms soliton solutions into lump solutions directly and consistently. This method ensures stability and localization, maintains a clear connection with soliton theory, and allows for deriving higher-order lump solutions, which the ansatz method cannot achieve.

The interaction between lumps and other nonlinear waves, including soliton and breather [3, 15, 20], is an active research area, with a particular focus on both elastic and inelastic collisions. However, there is still much to understand about the movement of lumps before and after collisions, phase shifts in lumps, and the trajectory equations governing their motion. Additionally, it is worth investigating other forms of interaction between lump waves and other waves, such as scenarios where they never collide or always collide and never separate.

In recent years, the study of the KP equation has remained a focal point of research, leading to its extensive application across various disciplines. In ocean fluid mechanics [8], the KP equation is employed to model vortical circulation and the propagation of ocean waves in spatial domains. In plasma physics [13], it is utilized for the generation and detection of plasma acoustic waves, playing a crucial role in both space exploration and industrial processes.

Based on the KP equation, Fokas [4] constructed the following $(4+1)$-dimensional equations

$$U_{x_2,t} = \frac{1}{4}(\partial_{x_1}^3 \partial_{x_2} - \partial_{x_1} \partial_{x_2}^3)U - \frac{3}{2}\partial_{x_1}\partial_{x_2}(U^2) + \frac{3}{2}\partial_{y_1}\partial_{y_2}U, \tag{1}$$

$$U_{x_1,t} = \frac{1}{16}(\partial_{x_1}^4 - 6\partial_{x_1}^2\partial_{x_2}^2 + \partial_{x_2}^4)U + \frac{3}{4}(\partial_{x_2}^2 - \partial_{x_1}^2)(P^2) + \frac{3}{4}(\partial_{y_1}^2 - \partial_{y_2}^2)U. \tag{2}$$

Akinyemi in [2] has reduced these equations to the $(2+1)$-dimensional form through the application of transformations

$$t = t, \quad x = ax_1 + bx_2, \quad y = cy_1 + dy_2, \tag{3}$$

where a, b, c, and d were arbitrary real constants. By combining the resulting equations, the new equation was formed as

$$(a+b)U_{xt} - \frac{1}{16}(a^4 + 4a^3b - 6a^2b^2 - 4ab^3 + b^4)U_{xxxx} - \frac{3}{4}(b^2 - 2ab - a^2)(U^2)_{xx}$$

$$- \frac{3}{4}(c^2 + 2cd - d^2)U_{yy} = 0. \tag{4}$$

Thus, the resulting $(2+1)$-dimensional Eqs. from transformation (3), together with Eq. (4), were generalized in the following manner:

$$\gamma_1 U_{xt} + \gamma_2 (U^2)_{xx} + \gamma_3 U_{xxxx} + \gamma_4 U_{yy} = 0. \tag{5}$$

The author in [2] has modified the equation by adding the $\gamma_5 U_{xx}$ term, resulting in the following extended $(2+1)$-dimensional eKP equation:

$$\gamma_1 U_{xt} + \gamma_2 (U^2)_{xx} + \gamma_3 U_{xxxx} + \gamma_4 U_{yy} + \gamma_5 U_{xx} = 0, \tag{6}$$

where $U = U(x,y,t)$ is an unknown differentiable function, and γ_i, $i = 1,\ldots,5$ are real arbitrary parameters. The term $\gamma_5 U_{xx}$ introduces an additional diffusion effect, which alters the rate of spatial spreading of the wave. This term adjusts the model to better capture physical phenomena such as enhanced dissipation or dispersion not accounted for in the original equation (5). The eKP Eq. (6) finds applications in nonlinear wave phenomena, plasma physics, optical fiber communications, fluid dynamics, and mathematical physics. Ref. [2] explores the integrability and soliton solutions for Eq. (6). The Painlev test is utilized to assess their integrability, and it is found that the equation successfully passes the Painlevé test.

Our motivation is to deepen the understanding of nonlinear wave solutions to the eKP equation (6), which could advance theoretical insights and improve practical applications in fields such as fluid mechanics and plasma physics. The focus of this study is on obtaining exact solutions for Eq. (6) using the Hirota bilinear technique. This approach provides soliton, lump, and hybrid solutions, including soliton-lump and breather-lump configurations.

The novelty of our work lies in tracking the trajectory of lump waves before and after collisions with other wave types. Specifically, we establish and clarify the conditions under which lump waves either avoid interactions with other waves or, if collisions occur, maintain their original state throughout the process.

The paper is organized as follows: Section 2 delves into the Hirota bilinear representation and soliton solution of Eq. (6). In Section 3, the focus shifts to the N-lump solution and its dynamics. Moving on to Section 4, we examine hybrid solutions of lump waves and soliton and breather waves, along with the trajectory of the lump wave before and after the interaction. Finally, Section 5 presents the conclusions.

2 $N-$soliton solution

In this section, we aim to construct an $N-$soliton solution to Eq. (6). We define the phase Φ_i in Eq. (6) as $\Phi_i = k_i x + p_i y - w_i t$, where w_i is the dispersion coefficient and k_i and p_i are real parameters. Substituting $U(x,y,t) = e^{\Phi_i}$ into the linear terms of Eq. (6), we obtain:

$$w_i = \frac{k_i^4 \gamma_3 + k_i^2 \gamma_5 + p_i^2 \gamma_4}{k_i \gamma_1}. \tag{7}$$

Based on the leading order behavior and coefficients in Painlevé analysis for the equation in [2], we consider the transformation $U(x,y,t) = \varepsilon(\ln f)_{xx}$, where ε and f are constants and an auxiliary function, respectively. Applying this transformation to Eq. (6) with $f(x,y,t) = 1 + e^{\Phi_i}$ and using (7), we solve for ε, resulting in $\varepsilon = \frac{6\gamma_3}{\gamma_2}$. Therefore, the transformation can be expressed as:

$$U = \frac{6\gamma_3}{\gamma_2} \ln(f)_{xx}. \tag{8}$$

Substituting (8) into (6) yields a bilinear equation in $f(x,y,t)$ as:

$$\left(\gamma_1 D_x D_t + \gamma_3 D_x^4 + \gamma_4 D_y^2 + \gamma_5 D_x^2 \right) f.f = 0. \tag{9}$$

where operator D_{xi} is defined as [7]

$$D_x^p D_y^q D_t^v f(x,y,t) g(x,y,t) = (\partial_x - \partial_{x'})^p (\partial_y - \partial_{y'})^q (\partial_t - \partial_{t'})^v [f(x,y,t)g(x',y',t')]\big|_{x=x',y=y',t=t'}. \tag{10}$$

Then, we choose the function f in the form

$$f = \sum_{\mu \in \{0,1\}^N} \exp\left(\sum_{i=1}^{N} \mu_i \chi_i + \sum_{i<j}^{N} \mu_i \mu_j \ln \Upsilon_{ij}\right), \tag{11}$$

where $\sum_{\mu \in \{0,1\}^N}$ represents the summation over all possible combinations of $\mu_j, \mu_s = 0,1,\ j,s = 1,2,\ldots,N$, and the wave variables are

$$\chi_i = k_i x + p_i y + w_i t + \phi_i. \tag{12}$$

As a result, the dispersion relation and the phase shifts are listed below, respectively.

$$w_i = -\frac{\gamma_3 k_i^4 + k_i^2 \gamma_5 + \gamma_4 p_i^2}{k_i \gamma_1}, \tag{13}$$

$$\Upsilon_{i,j} = \frac{3k_i^2 k_j^4 \gamma_3 - 6k_i^3 k_j^3 \gamma_3 + (3k_i^4 \gamma_3 - p_i^2 \gamma_4) k_j^2 + 2k_i k_j p_i p_j \gamma_4 - k_i^2 p_j^2 \gamma_4}{3k_i^2 k_j^4 \gamma_3 + 6k_i^3 k_j^3 \gamma_3 + (3k_i^4 \gamma_3 - p_i^2 \gamma_4) k_j^2 + 2k_i k_j p_i p_j \gamma_4 - k_i^2 p_j^2 \gamma_4}. \tag{14}$$

By incorporating formulas (13) and (14) into the function f and then applying it to the logarithmic transformation, an $N-$soliton solution to Eq. (6) can be derived.

3   Lump waves

The objective of this section is to offer a comprehensive explanation of how the asymptotic behavior of the soliton solution (11) results in the formation of lump waves. By meticulously choosing appropriate values for these parameters, one can create wave functions that demonstrate the desired lump-like behavior. These parameters significantly influence the characteristics of the resulting lump solution, including its amplitude, velocity, and position.

To obtain Nth-order lump solutions, we apply the long wave limit while considering the following conditions in N-soliton solution (11).

$$\begin{aligned} N = 2m, \ \ k_i = K_i \varepsilon, \ \ p_i = P_i \varepsilon, \ \ e^{\phi_i} = -1, \ \ \varepsilon \to 0, \\ K_1 = K_2^*, \ldots, K_{2m-1} = K_{2m}^* \ P_1 = P_2^*, \ldots, P_{2m-1} = P_{2m}^*. \end{aligned} \tag{15}$$

The notation $\varepsilon \to 0$ indicates that, after substituting the revised values of the parameters k_i and p_i into expression (11), an evaluation is performed to determine the limiting behavior of the resulting function. All these explanations can be summarized in the following theorem.

Theorem 1. *The comprehensive solutions for the N-th order lump can be expressed as the subsequent form.*

$$U_L^{(N)} = \frac{6\gamma_3}{\gamma_2} \ln(f_N)_{xx}, \tag{16}$$

where the function f_N is represented by the following expression.

$$f_N = \prod_{s=1}^{N} \theta_s + \frac{1}{2}\sum_{j,s}^{N} B_{js} \prod_{p\neq j,s}^{N} \theta_p + \cdots + \frac{1}{m!2^m} \sum_{l,s,\ldots,r,n}^{N} \overbrace{B_{ls}B_{jk}\cdots B_{mn}}^{m} \prod_{q\neq l,s,\ldots,r,n}^{N} \theta_q + \cdots, \tag{17}$$

and

$$\theta_i = -\frac{\left(K_i^2\gamma_5 + P_i^2\gamma_4\right)t}{K_i\gamma_1} + xK_i + yP_i, \quad B_{ij} = \frac{12K_i^3K_j^3\gamma_3}{\gamma_4\left(K_iP_j - K_jP_i\right)^2}. \tag{18}$$

Proof. The first two solutions of the N-soliton solution (11) are given by the following form:

$$f_1 = 1 + e^{\chi_1}, \tag{19}$$
$$f_2 = 1 + e^{\chi_1} + e^{\chi_2} + \Upsilon_{12}e^{\chi_1+\chi_2}. \tag{20}$$

The method for obtaining rational solutions from these soliton solutions depends on the flexibility of choosing the phase constant ϕ_i. For instance, by setting $\phi_1 = \mathbf{i}\pi$, and adjusting the parameters as $k_1 = K_1\varepsilon$ and $p_1 = P_1\varepsilon$, we can rewrite Eq. (19) in the following form:

$$f_1 = 1 - e^{\eta_1}, \tag{21}$$

which corresponds to a singular soliton solution

$$U = -\frac{6\gamma_3\varepsilon^2 K_1^2}{\gamma_2}\frac{\left(\cosh(\eta_1) - \sinh(\eta_1)\right)}{\left(-1 + \cosh(\eta_1) - \sinh(\eta_1)\right)^2} \tag{22}$$

with

$$\eta_1 = \varepsilon K_1 x + \varepsilon P_1 y - \frac{\left(\varepsilon^4 K_1^4\gamma_3 + \varepsilon^2 K_1^2\gamma_5 + \varepsilon^2 P_1^2\gamma_4\right)}{\varepsilon K_1\gamma_1}t.$$

Reaching the "*long wave*" limit $K_1 \to 0$ in Eq. (21) results in

$$f_1 = -\varepsilon\theta_1 + O(\varepsilon^2), \tag{23}$$

where θ_1 is described in (18). We can introduce an arbitrary phase factor to θ_i. Given that U is defined by (8), we have derived the following rational solution

$$U = -\frac{6\gamma_3 K_1^2}{\gamma_2\theta_1^2}, \tag{24}$$

which gives a singular solution.

For the two-soliton solution given in Eq. (20), we set $\phi_i = \mathbf{i}\pi$, $i = 1,2$ and $\varepsilon \to 0$, with $K_1/K_2 = O(1)$ and $\varepsilon P_i = O(1)$. Then, by observing

$$\Upsilon_{12} = 1 + \frac{12K_1^3K_2^3\gamma_3}{\gamma_4\left(K_1P_2 - K_2P_1\right)^2} + O(\varepsilon^3), \tag{25}$$

we find

$$
\begin{aligned}
f_2 = \varepsilon^2 \Bigg[& \frac{\left(K_1^2\gamma_5 + P_1^2 s_4\right)\left(K_2^2\gamma_5 + P_2^2 s_4\right) t^2}{K_1 s_1^2 K_2} + \Big[\Big(-\frac{K_1\left(K_2^2\gamma_5 + P_2^2 s_4\right)}{K_2 s_1} - \frac{\left(K_1^2\gamma_5 + P_1^2 s_4\right) K_2}{K_1 s_1} \Big) x \\
& + \Big(-\frac{P_1\left(K_2^2\gamma_5 + P_2^2 s_4\right)}{K_2 s_1} - \frac{\left(K_1^2\gamma_5 + P_1^2 s_4\right) P_2}{K_1 s_1} \Big) y \Big] t + K_2 K_1 x^2 + (K_1 P_2 + K_2 P_1)\, yx + P_1 P_2 y^2 \\
& + \frac{12 K_1^3 K_2^3 \gamma_3}{\gamma_4 \left(K_1 P_2 - K_2 P_1\right)^2} + O(\varepsilon) \Bigg] \\
= \varepsilon^2 \Big[& \theta_1 \theta_2 + \frac{12 K_1^3 K_2^3 \gamma_3}{\gamma_4 \left(K_1 P_2 - K_2 P_1\right)^2} + O(\varepsilon) \Big]
\end{aligned}
\tag{26}
$$

Taking into account that the solution (8) remains invariant under the transformation $f \to \varepsilon^2 f$, we can rewrite f_2 as:

$$
f_2 = \theta_1 \theta_2 + B_{1,2},
\tag{27}
$$

where θ_i and $B_{i,j}$ are represented in (18). By applying the logarithmic transformation (8) and setting $K_1 = K_2^*$ and $P_1 = P_2^*$, a real-valued lump solution can be constructed.

This approach to obtaining rational solutions can be generalized to the N-soliton case given in (11). Initially, we set $\phi_i = \mathbf{i}\pi$ for each term in (11). As a result, f_N transforms into the following expression:

$$
f_N = \sum_{\mu \in \{0,1\}^N} \prod_{i=1}^N (-1)^{\mu_i} \exp(\mu_i \chi_i) \times \prod_{i<j}^N \exp(\mu_i \mu_j \ln(\Upsilon_{ij})).
\tag{28}
$$

For $k_1 = \varepsilon K_1$ and $p_1 = \varepsilon P_1$, it is evident that

$$
f_N \big|_{\varepsilon=0} = \sum_{\mu \in \{0,1\}^N} (-1)^{\mu_i} f_{N-1} = 0,
\tag{29}
$$

where f_{N-1} is an $N-1$-soliton solution with parameters, $k_2, p_2, k_3, p_3, \ldots, k_N, p_N$.

Given the symmetric nature of f_N with respect to εk_i and εp_i, we observe that f_N can be factored by ε^i, $i = 1, 2, \ldots, N$. Consequently, when expanding f_N in powers of ε, the leading terms in (28) must be at least of the order ε^N. Taking the limit as $\varepsilon \to 0$ and assuming all k_i and p_i share the same asymptotic behavior, we obtain

$$
f_N = \sum_{\mu \in \{0,1\}^N} \prod_{i=1}^N (-1)^{\mu_i}(1 + \varepsilon \mu_i \theta_i) \times \prod_{i<j}^N (1 + \varepsilon^2 \mu_i \mu_j B_{ij}) + O(\varepsilon^{N+1}).
\tag{30}
$$

The dominant terms in (30) are those of order ε^i, $i = 1, 2, \ldots, N$ in $\prod_{i=1}^N (1 + \varepsilon \theta_i) \prod_{i<j}^N (1 + \varepsilon^2 B_{ij})$. Consequently, a rational solution derived from the long-wave limit of the N-soliton solution can be formulated as (17). To derive a real-valued lump solution, one should set $K_{2m-1} = K_{2m}^*$ and $P_{2m-1} = P_{2m}^*$ for $m = \frac{N}{2}$ within the general solution given by (17).   □

Proposition 1. *The m-th lump wave in the solution* (16) *is characterized by the following properties:*

- *The trajectory of the m-th lump wave is given by*

$$y = \frac{\gamma_4 \left(K_{2m-1}P_{2m} + K_{2m}P_{2m-1}\right)}{K_{2m-1}K_{2m}\gamma_5 - P_{2m-1}P_{2m}\gamma_4} x, \tag{31}$$

- *The amplitude formula is*

$$A_m^{[N]} = \frac{\gamma_4 \left(K_{2m-1}P_{2m} - K_{2m}P_{2m-1}\right)^2}{\gamma_2 K_{2m-1}^2 K_{2m}^2}, \tag{32}$$

- *Velocity of the lump wave are determined by*

$$V_m^{[N]} = \sqrt{\frac{\left(K_{2m-1}K_{2m}\gamma_5 - P_{2m-1}P_{2m}\gamma_4\right)^2}{K_{2m}^2\gamma_1^2 K_{2m-1}^2} + \frac{\gamma_4^2 \left(K_{2m-1}P_{2m} + K_{2m}P_{2m-1}\right)^2}{K_{2m}^2\gamma_1^2 K_{2m-1}^2}}. \tag{33}$$

Proof. To determine the trajectory of each peak in the N-lump solution (16), start by setting the partial derivatives of the solution with respect to x and y to zero. This yields a system of equations that can be solved for x and y. Next, compute the value of t from the x-solution, and then substitute this value into the y-solution. This process will provide the trajectory of each peak, which is described by (31).

Furthermore, by substituting the values of x and y from the previously discussed system of equations into the N-lump solution (16), we can determine the amplitude of the peak as described in equation (32). We can easily determine the peak velocity by differentiating the aforementioned temporal-spatial equation with respect to t, as shown in (33). □

To achieve a single lump, one can substitute $N = 2$ into the formula (17). This substitution results in the expression of U_1 as shown below:

$$U_1 = \frac{6\gamma_3}{\gamma_2} \ln(\theta_1 \theta_2 + B_{1,2})_{xx}, \tag{34}$$

where, θ_i and $B_{i,j}$ are represented in (18). Figure 1 (a) illustrates the dynamics of the one-lump solution (34). With specific parameter selections, the amplitude and velocity of the wave are $A_1^{[1]} = 3.43.408284$ and $V_1^{[1]} = 0.6369421$, respectively. Furthermore, Figure 1 (d) displays the trajectory of the wave over time. For $N = 4, 6$, the two and three-lump solutions are presented in Figure 1 (b,c). As observed in the figure, the two-lump solution exhibits two separate peaks that move away from each other as time increases. The amplitude and velocity of the first wave are $V_1^{[2]} = 5.4589$ and $A_1^{[2]} = 1.583$, respectively, while for the second wave, these values are $V_2^{[2]} = 1.36$ and $A_2^{[2]} = 1.498$, respectively. Moreover, in the three-lump solution, there are three separate peaks with the following amplitudes and velocities: $V_1^{[3]} = 0.66899$, $V_2^{[3]} = 4.60977$, $V_3^{[3]} = 3.2811$ and $A_1^{[3]} = 3.07$, $A_2^{[3]} = 6.25$, $A_3^{[3]} = 8.134$. Additionally, the trajectory of each peak in the aforementioned solution is clearly represented in Figure 1 (e,f).

4 Interaction between lump and soliton waves

In this section, we delve into the development of a unique hybrid solution that merges both lump and other wave forms. This hybrid solution is attained through the utilization of the long wave limit method [1]
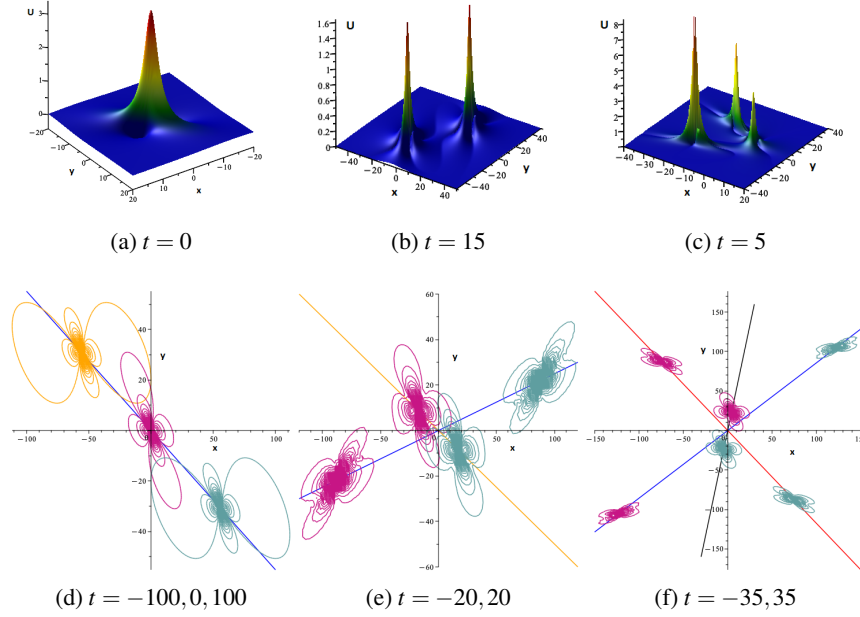
Figure 1: **Panels (a, d):** One-lump soution with, $K_1 = K_2^* = 2 + 3\mathrm{I}, P_1 = P_2^* = 4$. Trajectory of lump $y = -\frac{16}{29}x$ (blue line). **Panels (b, e):** Two-lump solution with, $K_1 = K_2^* = 2 + 4\mathrm{I}, K_3 = K_4^* = 1 + 4\mathrm{I}, P_1 = P_2^* = 3, P_3 = P_4^* = 3$. Trajectory of the first lump $y = -\frac{24}{13}x$ (orange line) and the second lump $y = \frac{15}{8}x$ (blue line). **Panels (c, f):** Three-lump solution with, $K_1 = K_2^* = 1.5 + 4.0\mathrm{I}, K_3 = K_4^* = -1 + \mathrm{I}, K_5 = K_6^* = 2 + 2\mathrm{I}, P_1 = P_2^* = 4, P_3 = P_4^* = 3, P_5 = P_6^* = 5$. Trajectory of the first lump $y = \frac{6}{7}x$ (blue line), the second lump $y = -\frac{20}{17}x$ (red line) and the third lump $y = \frac{19}{5}x$ (black line). For the same selection of $\gamma_5 = 1, \gamma_1 = 1, \gamma_2 = 1, \gamma_3 = -1, \gamma_4 = 1$.

based on the *N*-soliton solution (11). Employing this method allows us to derive a range of semi-rational solutions that incorporate blends of lumps and soliton lines, as well as a combenation of lumps and breathers.

Proposition 2. *To obtain a hybrid solution comprising $\mathscr{L}$ lump waves and $\mathscr{S}$ soliton waves, we can take the long wave limit with the following restrictions in Eq.* (11).

$$N = 2\mathscr{L} + \mathscr{S}, \quad m = 1, 2, ..., 2\mathscr{L}, \quad k_m = K_m \varepsilon, \quad p_m = P_m \varepsilon, \quad \phi_m = \pi i, \quad \varepsilon \to 0, \tag{35}$$
$$K_1 = K_2^*, K_3 = K_4^*, \ldots, K_{2\mathscr{L}-1} = K_{2\mathscr{L}}^*, \quad P_1 = P_2^*, P_3 = P_4^*, \ldots, P_{2\mathscr{L}-1} = P_{2\mathscr{L}}^*.$$

Proof. The proof of this proposition is essentially the same as that of Theorem 1, with the key difference being that the parameters $k_{\mathscr{S}}$ and $p_{\mathscr{S}}$ remain unchanged. □

Studying the trajectory equations of lump waves and soliton lines before and after collision [20], enhances our understanding of their complex interaction. In the following, we discuss this issue further.

Theorem 2. *For the mixed solution comprising $\mathscr{L}$-lump waves and $\mathscr{S}$-soliton lines, under the condition $\lambda_3, \lambda_4, \ldots, \lambda_{2+\mathscr{S}} \neq 0$, and based on conditions* (35), *the trajectory equations of an arbitrary lump wave*

are as below:

$$(x_b, y_b) = \left(X + \sum_{s=2\mathscr{L}+1}^{N} h_b(\lambda_s)\kappa_s, \, Y + \sum_{s=2\mathscr{L}+1}^{N} h_b(\lambda_s)\vartheta_s \right),$$

$$(x_a, y_a) = \left(X + \sum_{s=2\mathscr{L}+1}^{N} h_a(\lambda_s)\kappa_s, \, Y + \sum_{s=2\mathscr{L}+1}^{N} h_a(\lambda_s)\vartheta_s \right), \tag{36}$$

where

$$(X, Y) = \left(\frac{(K_{2m-1}K_{2m}\gamma_5 - P_{2m-1}P_{2m}\gamma_4)}{K_{2m}\gamma_1 K_{2m-1}}t, \, \frac{\gamma_4\left(K_{2m-1}P_{2m} + K_{2m}P_{2m-1}\right)}{K_{2m}\gamma_1 K_{2m-1}}t \right), \tag{37}$$

$$\kappa_s = \frac{-B_{2m-1,s}P_{2m} + B_{2m,s}P_{2m-1}}{K_{2m-1}P_{2m} - K_{2m}P_{2m-1}}, \quad \vartheta_s = \frac{B_{2m-1,s}K_{2m} - B_{2m,s}K_{2m-1}}{K_{2m-1}P_{2m} - K_{2m}P_{2m-1}}. \tag{38}$$

$$\lambda_s = \frac{-K_{2m-1}K_{2m}k_s^4\gamma_3 - P_{2m-1}P_{2m}k_s^2\gamma_4 + p_s\gamma_4\left(K_{2m-1}P_{2m} + K_{2m}P_{2m-1}\right)k_s - K_{2m-1}K_{2m}p_s^2\gamma_4}{K_{2m}\gamma_1 K_{2m-1}k_s}, \tag{39}$$

$$h_b(x) = \begin{cases} 1, & x < 0 \\ 0, & x \geq 0 \end{cases}, \quad h_a(x) = \begin{cases} 0, & x \leq 0 \\ 1, & x > 0 \end{cases}, \tag{40}$$

For $1 \leq i < j \leq 2\mathscr{L}$, $B_{i,j}$ are presented in (18) and for $1 \leq i \leq 2\mathscr{L}$ and $j > 2\mathscr{L}$ it is as fallows:

$$B_{i,j} = \frac{12K_i^3 k_j^3 \gamma_3}{3K_i^2 k_j^4 \gamma_3 - K_i^2 p_j^2 \gamma_4 + 2K_i P_i k_j p_j \gamma_4 - P_i^2 k_j^2 \gamma_4}. \tag{41}$$

The change in the phase of the lump wave before and after the collision can be expressed as

$$\Delta_b = \sum_{s=2\mathscr{L}+1}^{N} sign(\lambda_s)\Delta_{bs}, \tag{42}$$

where

$$\Delta_{bs} = \frac{-B_{2m,s}K_{2m-1}^2 K_{2m}\gamma_5 + B_{2m-1,s}\left(K_{2m}^2\gamma_5 + P_{2m}^2\gamma_4\right)K_{2m-1} - B_{2m,s}K_2 P_{2m-1}^2\gamma_4}{\left(K_{2m-1}P_{2m} - K_{2m}P_1\right)\left(K_{2m-1}K_{2m}\gamma_5 - P_{2m-1}P_{2m}\gamma_4\right)}. \tag{43}$$

However, the amplitude and velocity of the peak do not change before and after the collision, and they are represented by formula (32) and (33), respectively.

Proof. To prove this theorem, we consider solutions that consist of a lump wave and a soliton line. The proof for the other situations remains the same, and we will omit their proof for brevity.

First, let us consider a mixed solution consisting of a lump wave and a soliton wave based on the conditions (35) as follows:

$$U_{LS}^{(1)} = \frac{6\gamma_3}{\gamma_2}\ln(f_{LS}^{(1)})_{xx}, \tag{44}$$

with

$$f_{LS}^{(1)} = \theta_1\theta_2 + B_{1,2} + (B_{1,3}B_{2,3} + \theta_2 B_{1,3} + \theta_1 B_{2,3} + \theta_1\theta_2 + B_{1,2})\,e^{\chi_3}. \tag{45}$$

Regarding the lump wave's path in (31), we assume it follows a straight line before and after collision. Hence, the function $f_{LS}^{(1)}$ is bound by the subsequent conditions

$$(x,y) = \left(\frac{(K_1 K_2 \gamma_5 - P_1 P_2 \gamma_4)}{K_2 \gamma_1 K_1} t + c_1, \frac{\gamma_4\,(K_1 P_2 + K_2 P_1)}{K_2 \gamma_1 K_1} t + c_2 \right). \tag{46}$$

Substituting (46) into (45) yields

$$f_{LS}^{(1)} = e^{t\lambda_3 + \beta_3}\,(B_{1,3}B_{2,3} + B_{1,3}\zeta_2 + B_{2,3}\zeta_1 + \zeta_1\zeta_2 + B_{1,2}) + B_{1,2} + \zeta_1\zeta_2,$$

where

$$\zeta_1 = K_1 c_1 + P_1 c_2, \quad \zeta_2 = K_2 c_1 + P_2 c_2, \quad \beta_3 = c_1 k_3 + c_2 p_3 + \phi_3.$$

When $\lim_{t\to\pm\infty} f_{LS}^{(1)}$ we can derive the following approximate expressions.

Case I: For $\lambda_3 > 0$,

$$f_b = B_{1,2} + \zeta_1\zeta_2, \quad f_a = B_{1,3}B_{2,3} + B_{1,3}\zeta_2 + B_{2,3}\zeta_1 + \zeta_1\zeta_2 + B_{1,2}. \tag{47}$$

By substituting the values of c_1 and c_2 from (46) into (47), we obtain the following expressions:

$$f_b = \theta_1\theta_2 + B_{1,2}, \quad f_a = B_{1,3}B_{2,3} + B_{1,3}\theta_2 + B_{2,3}\theta_1 + \theta_1\theta_2 + B_{1,2}. \tag{48}$$

These expressions feature the functions f_b and f_a, representing the states of the lump peak and soliton before and after the collision, respectively. It is crucial to highlight that these functions adhere to the bilinear Eq. (9).

Substituting (48) into (44) and equating the derivatives of the solutions with respect to x and y to zero allows us to ascertain the trajectories of the peak before and after the collision:

$$(x_b, y_b) = \left(\frac{(K_1 K_2 \gamma_5 - P_1 P_2 \gamma_4)}{K_2 \gamma_1 K_1} t, \frac{\gamma_4\,(K_1 P_2 + K_2 P_1)}{K_2 \gamma_1 K_1} t \right),$$

$$(x_a, y_a) = \left(\frac{(K_1 K_2 \gamma_5 - P_1 P_2 \gamma_4)}{K_2 \gamma_1 K_1} t + \frac{-B_{1,3}P_2 + B_{2,3}P_1}{K_1 P_2 - K_2 P_1}, \frac{\gamma_4\,(K_1 P_2 + K_2 P_1)}{K_2 \gamma_1 K_1} t + \frac{B_{1,3}K_2 - B_{2,3}K_1}{K_1 P_2 - K_2 P_1} \right), \tag{49}$$

In this scenario, the validity of expressions (36) is confirmed. Additionally, the phase change (42) can be easily determined by comparing the peak's trajectories before and after the collision, without involving the time parameter.

When substituting the values of x_b, y_b, x_a, and y_a into (44), it becomes apparent that the peak's amplitude remains unchanged following the collision

Case II: Let us consider the scenario where $\lambda_3 < 0$. The proof follows a similar approach to the previous one, but with a notable distinction: $\lim_{t\to\pm\infty} f_{LS}^{(1)}$ yields the following expressions:

$$f_b = B_{1,3}B_{2,3} + B_{1,3}\zeta_2 + B_{2,3}\zeta_1 + \zeta_1\zeta_2 + B_{1,2}, \quad f_a = B_{1,2} + \zeta_1\zeta_2. \tag{50}$$

In this particular case, the trajectory after the collision precisely mirrors the trajectory before the collision in the previous case. Conversely, the trajectory before the collision in this case aligns with the trajectory after the collision in Case I. $\qquad\square$

Corollary 1. *The condition for the avoidance of collision or the preservation of wave states during the interaction between a lump wave and a soliton wave arises when $\lambda_s = 0$. Simply put, this condition is met when the velocity of the lump wave matches the velocity of the soliton line, given by: $V_{\mathscr{L}} = V_{\mathscr{S}}$, where*

$$V_{\mathscr{S}} = \left[-\frac{w_i k_i}{k_i^2 + p_i^2}, -\frac{w_i p_i}{k_i^2 + p_i^2} \right],$$

and w_i, $V_{\mathscr{L}}$, and λ_s are defined in (13), (33), and (39), respectively.

We investigate three scenarios of wave collisions for clearer insight. Firstly, we analyze the collision between a soliton wave and a lump wave. Secondly, we explore the collision of two soliton waves and a lump wave. Lastly, we examine the collision between one soliton wave and two lump waves.

Example 1. The interaction between a lump wave and a soliton wave solution (44), is illustrated in Figure 5. Upon evaluating Eq. (39), we ascertain $\lambda_3 = -4.0771635 < 0$. Consequently, we deduce $h_b(\lambda_3) = 1$ and $h_a(\lambda_3) = 0$. Thus, the lump wave initially follows the trajectory $y = 0.3741x - 0.7167$ before colliding with the soliton wave. However, post-collision, the lump wave alters its course, shifting to $y = 0.3741x$. Additionally, the change in phase, denoted by $\Delta_{b3} = 0.7167$. Notably, the lump wave maintains consistent velocity and amplitude pre and post collision, with $V_1^{[1]} = 0.5386$ and $A_1^{[1]} = 1.964$. Moreover, based on Corollary 1, specific conditions are established to ensure that the interaction between lump and soliton waves never results in a collision. This phenomenon is illustrated in Figure 3.

(a) $t = -10$ (b) $t = 0$ (c) $t = 10$ (d)
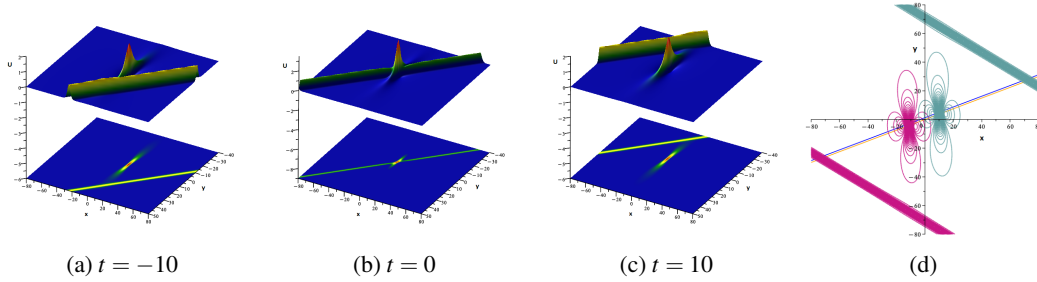
Figure 2: Superposition of a lump and a soliton wave with $K_1 = K_2^* = \frac{2}{7} - 3\mathrm{I}, P_1 = P_2^* = \frac{3}{2}, \gamma_5 = 1, k_3 = \frac{4}{5}, p_3 = \frac{4}{3}, \phi_3 = 0, \gamma_1 = 1, \gamma_2 = -1, \gamma_3 = -1, \gamma_4 = 2$. **Panel c:** Trajectory of lump before the interaction $y = 0.3741x - 0.7167$ (orange line) and after the interaction $y = 0.3741x$ (blue line) for $t = -20$ (crimson) and $t = 20$ (cadet blue).

Example 2. The solution represented by $U_{LS}^{(2)} = \frac{6\gamma_3}{\gamma_2} \ln(f_{LS}^{(2)})_{xx}$, where

$$\begin{aligned}
f_{LS}^{(2)} = {}& e^{\chi_3} \left(B_{1,3} B_{2,3} + B_{1,3} \theta_2 + B_{2,3} \theta_1 + \theta_1 \theta_2 + B_{1,2} \right) \\
& + e^{\chi_4} \left(B_{1,4} B_{2,4} + B_{1,4} \varpi_2 + B_{2,4} \theta_1 + \theta_1 \theta_2 + B_{1,2} \right) \\
& + \Upsilon_{3,4} e^{\chi_3 + \chi_4} \left(B_{1,3} B_{2,3} + B_{1,3} B_{2,4} + B_{1,3} \theta_2 + B_{1,4} B_{2,3} + B_{1,4} B_{2,4} \right. \\
& \left. + B_{1,4} \theta_2 + B_{2,3} \theta_1 + B_{2,4} \theta_1 + \theta_1 \theta_2 + B_{1,2} \right) \\
& + \theta_1 \theta_2 + B_{1,2},
\end{aligned} \tag{51}$$

(a) $t = -40$ (b) $t = 0$ (c) $t = 40$
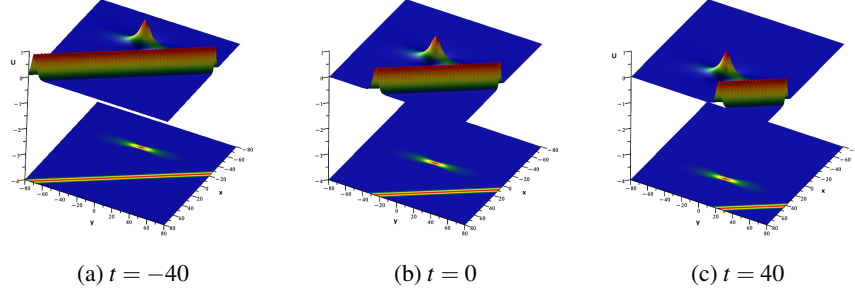
Figure 3: In the superposition of a lump and a soliton wave these waves nevere colid if: $K_1 = K_2^* = \frac{2}{7} - 3I, P_1 = P_2^* = \frac{3}{2}, \gamma_5 = 1, k_3 = \frac{4}{5}, p_3 = 0.5402102468 \phi_3 = -50, \gamma_1 = 1, \gamma_2 = -1, \gamma_3 = -1, \gamma_4 = 1.$

combines one lump wave and two solitons. This solution is shown in Figure 4 for various times. After computation, we confirm that $\lambda_3 = -1.834791667 < 0$ and $\lambda_4 = -1.37944 < 0$. Following theorem 2, the trajectories of the lump wave before and after the interaction are visually illustrated in Figure 4 (d), with the phase shift indicated by $\Delta_{b_3} = 0.3986457101$. Notably, the velocity and amplitude of the lump wave remain constant before and after the collision, with values of $V_1^{[2]} = 1.4422$ and $A_1^{[2]} = 6.48$, respectively.

(a) $t = -20$ (b) $t = 0$ (c) $t = 20$ (d)
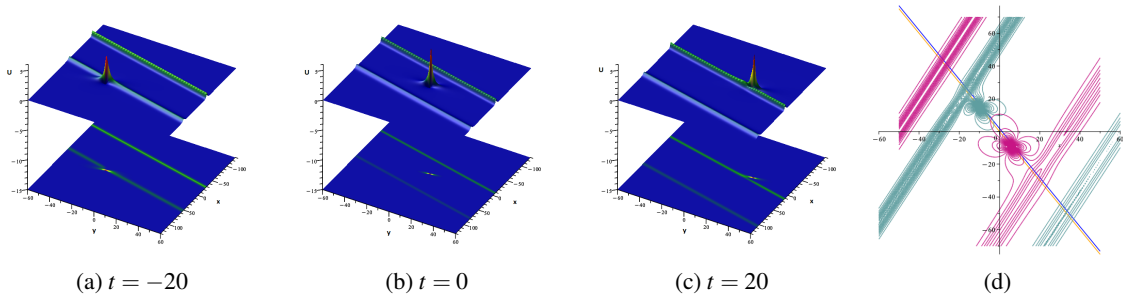
Figure 4: Superposition of a lump and two soliton waves with $K_1 = K_2^* = \frac{1}{2} - \frac{3I}{2}, P_1 = P_2^* = \frac{3}{2}, \gamma_5 = 1, k_3 = \frac{3}{4}, k_4 = \frac{1}{2}, p_3 = -\frac{2}{5}, \phi_3 = 30, \phi_4 = -20, \gamma_1 = 1, \gamma_2 = -1, \gamma_3 = -1, \gamma_4 = 2.$ **Panel c:** Trajectory of the lump before the interaction $y = -1.5x + 0.3986$ (orange line) and after the interaction $y = -1.5x$ (blue line). for $t = -10$ (crimson) and $t = 10$ (cadet blue).

Example 3. To achieve a composite solution involving two lump waves and a line soliton we set $N = 6$, $\mathscr{S} = 1$, and $\mathscr{L} = 2$ according to conditions (35). This results in the emergence of a novel solution denoted as $U_{LS}^{(3)}$, as depicted in Figure 5. For the first lump wave, we determine $\lambda_5 = \frac{-7}{10}$, while for the second lump wave, $\lambda_5 = \frac{11}{2}$. As per theorem 2, the trajectories before and after the collision of the first and second lump waves are delineated in Figure 5 (c). The velocity and amplitude of the first lump wave are quantified as $V_1^{[3]} = 5.4589$ and $A_1^{[3]} = 2.88$, respectively. Correspondingly, for the second lump wave, we compute $A_2^{[3]} = 0.72$ and $V_2^{[3]} = 1.36$.

(a) $t = -20$ (b) $t = 0$ (c) $t = 20$ (d)
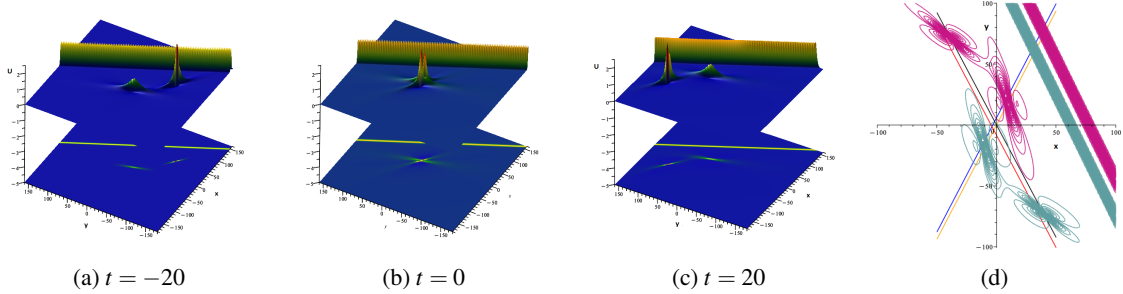
Figure 5: Superposition of two lumps and a soliton wave with $K_1 = K_2^* = 2 - \mathrm{I}, K_3 = K_4^* = 1 - \mathrm{I}, P_1 = P_2^* = 3, P_3 = \frac{3}{5}, P_4 = \frac{3}{5}, \gamma_5 = 1, k_5 = 1, p_5 = \frac{1}{2}, \phi_5 = -70, \gamma_1 = 1, \gamma_2 = -1, \gamma_3 = -1, \gamma_4 = 2$. **Panel c:** Trajectory of the first lump before the interaction $y = 1.875x + 5.9343$ (orange line) and after the interaction $y = 1.875x$ (blue line). Trajectory of the second lump before the interaction $y = -1.8461x - 8.405$ (black line) and after the interaction $y = -1.8461x$ (red line) for $t = -15$ (crimson) and $t = 15$ (cadet blue).

In this part, we present a method for examining the interaction between lump waves and breather waves. To obtain a combined solution comprising $\mathscr{L}$ lump waves and $\mathscr{B}$ breather waves for Eq. (6), we start by setting $N = 2(\mathscr{B} + \mathscr{L})$ and then impose specific constraints on the N-soliton solution (11) as follows:

$$1 \leq m \leq 2\mathscr{L}, \ k_{2m-1} = k_{2m}^* = K_{2m-1}\varepsilon, \quad p_{2m-1} = p_{2m}^* = P_{2m-1}\varepsilon, \quad \phi_{2m-1} = \phi_{2m} = \pi\mathbf{i}, \ \varepsilon \to 0,$$
$$k_{2\mathscr{L}+1} = k_{2\mathscr{L}+2}^*, ..., k_{2\mathscr{L}+2\mathscr{B}-1} = k_{2\mathscr{L}+2\mathscr{B}}^*, \quad p_{2\mathscr{L}+1} = p_{2\mathscr{L}+2}^*, ..., p_{2\mathscr{L}+2\mathscr{B}-1} = q_{2\mathscr{L}+2\mathscr{B}}^*,$$
$$\phi_{2\mathscr{L}+1} = \phi_{2\mathscr{L}+2}^*, ..., \phi_{2\mathscr{L}+2\mathscr{B}-1} = \phi_{2\mathscr{L}+2\mathscr{B}}^*. \tag{52}$$

In a similar manner as previously, we can formulate a theorem delineating the path followed by the lump wave before and after its interaction with the breather wave.

Proposition 3. *The equations governing the trajectory of a lump wave before and after colliding with breather waves for $\lambda_s \neq 0$ are listed as follows:*

$$(x_b, y_b) = \left(X + \sum_{s=2\mathscr{L}+1}^{N} h_b(Re(\lambda_s))\kappa_s, \ Y + \sum_{s=2\mathscr{L}+1}^{N} h_b(Re(\lambda_s))\vartheta_s \right),$$

$$(x_a, y_a) = \left(X + \sum_{s=2\mathscr{L}+1}^{N} h_a(Re(\lambda)_s)\kappa_s, \ Y + \sum_{s=2\mathscr{L}+1}^{N} h_a(Re(\lambda_s))\vartheta_s \right),$$

where X, Y, κ_s, ϑ_s, λ_s, h_b and h_a are given by Eqs. (37)-(40) and $Re(\lambda_s)$ denotes the real part of λ_s.

Proof. The proof is essentially the same as that of Theorem 2, with the key difference being that the constraints in (52) must be applied during the proof process. $\square$

Example 4. For $N = 4$, which corresponds to $\mathscr{L} = 1$ and $\mathscr{B} = 1$ according to conditions (52), a hybrid solution comprising a breather wave and a lump wave can be derived. To visually illustrate the collision between these waves, Figure 6 depicts the physical behavior of this interaction.

(a) $t = -10$ (b) $t = 0$ (c) $t = 10$ (d)
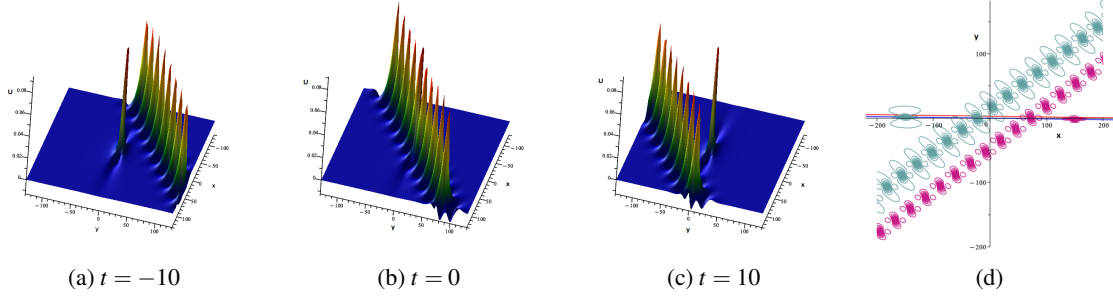
Figure 6: Superposition of a lump and a breather wave with $K_1 = K_2^* = \frac{3}{7} + \frac{1}{5}, P_1 = P_2^* = 1 - 2\mathrm{I}, \gamma_5 = 1, k_3 = k_4^* = \frac{1}{12} - \frac{1}{8}, p_3 = p_4^* = -\frac{1}{8} - \frac{1}{6}, \gamma_1 = 1, \gamma_2 = 3, \gamma_3 = 1, \gamma_4 = 1, \phi_3 = \phi_4^* = 0.$ **Panel c:** Trajectory of the lump before the interaction $y = -0.01196x - 0.01509$ (red line) and after the interaction $y = -0.01196x$ (blue line). for $t = -7$ (crimson) and $t = 7$ (cadet blue),

The collision behavior observed in the superposition of the lump and soliton, as explored in Corollary 1, similarly occurs here. That is, the lump wave and the breather wave either do not collide, or if they do, they remain in the same state.

Corollary 2. *When the condition $Re(\lambda_s) = 0$ is satisfied, lump and breather waves either do not collide or remain in a collided state. This condition signifies that the velocity of the lump wave equals the velocity of the breather wave, expressed as $V_{\mathscr{L}} = V_{\mathscr{B}}$, where*

$$V_{\mathscr{B}} = \left[-\frac{Re(w_i)Re(k_i)}{(Re(k_i))^2 + (Re(p_i)^2}, -\frac{Re(w_i)Re(p_i)}{(Re(p_i))^2 + (Re(p_i))^2} \right],$$

and w_i and $V_{\mathscr{L}}$ are defined in (13) and (33).

The collision between the lump wave and the breather wave, illustrated in Figure 7, occurs in such a way that the two waves pass through each other without any interference or interaction. This behavior is achieved through carefully chosen parameters that meet the conditions outlined in Corollary 2.

(a) $t = -1$ (b) $t = 0$ (c) $t = 1$
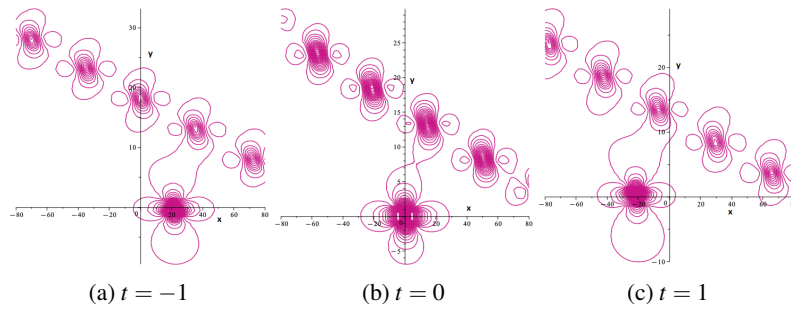
Figure 7: In the superposition of a lump and a breather wave these waves nevere colid if: $K_1 = K_2^* = \frac{3}{7} + \frac{1}{5}, P_1 = P_2^* = 1 - 2\mathrm{I}, \gamma_5 = 1, k_3 = k_4^* = \frac{1}{12} - \frac{1}{8}, p_3 = p_4^* = 0.6014984038 + 0.3775372501\,\mathrm{I}, \phi_3 = \phi_4^* = -10, \gamma_1 = 1, \gamma_2 = 3, \gamma_3 = 1, \gamma_4 = 1.$

5   Conclusion

In this study, we obtained an $N-$soliton solution for Eq. (6) to investigate the dynamics of lump waves. By leveraging the asymptotic behavior of soliton solutions and employing the long wave limit method, we successfully derived multiple lump solutions. We also examined the interactions between lump waves and other wave types, including soliton and breather waves. Notably, we calculated the trajectory of the peak before and after each collision and identified conditions under which the lump wave avoids collision with other waves. Furthermore, we demonstrated that if a collision occurs, the lump wave remains unchanged. Our research includes a comprehensive graphical analysis of the solutions, accompanied by detailed explanations of key parameters such as velocity, amplitude, and peak location for each wave.

In future work, it remains an open problem whether Eq. (6) can be effectively transformed into a stochastic PDE and solved using the variable coefficient third-degree generalized Abel equation method [5]. This approach could potentially reveal new insights and solutions, enhancing our understanding of complex nonlinear equations influenced by stochastic processes.

References

[1] M.J. Ablowitz, J. Satsuma, *Solitons and rational solutions of nonlinear evolution equations,* J. Math. Phys. **19** (1978) 2180–2186.

[2] L. Akinyemi, *Shallow ocean soliton and localized waves in extended (2+ 1)-dimensional nonlinear evolution equations,* Phys. Lett. A. **463** (2023) 1–24.

[3] J.S. Chen, Y. Hang, X. Lü, *Elastic collision between one lump wave and multiple stripe waves of nonlinear evolution equations,* Commun. Nonlinear Sci. Numer. Simul. **130** (2024) 1–17.

[4] A.S. Fokas, *Integrable nonlinear evolution partial differential equations in 4+ 2 and 3+ 1 dimensions,* Phys. Rev. Lett. **96** (2006) 1–9.

[5] M.S. Hashemi, *A variable coefficient third degree generalized Abel equation method for solving stochastic Schrödinger–Hirota model,* Chaos Solitons Fractals. **180** (2024) 1–8.

[6] R. Hirota, *Exact solution of the Kortewegde Vries equation for multiple collisions of solitons*, Phys. Rev. Lett. **27** (1971) 19–28.

[7] R. Hirota, *The Direct Method in Soliton Theory,* Cambridge University Press, 2004.

[8] I.M. Tarikul, M.A. Akter, S. Ryehan, J.F. Gómez, M.D. Akbar, *A variety of solitons on the oceans exposed by the Kadomtsev Petviashvili-modified equal width equation adopting different techniques,* J. Ocean Engin. Sci. **7** (2022) 528–535.

[9] S. Kumar, B. Mohan, *A generalized nonlinear fifth-order KdV-type equation with multiple soliton solutions: Painlevé analysis and Hirota Bilinear technique,* Phys. Scr. **97** (2022) 123–132.

[10] Y. Li, X. Hao, R. Yao, Y. Xia, Y. Shen, *Nonlinear superposition among lump soliton, stripe solitons and other nonlinear localized waves of the (2+ 1)-dimensional cpKP-BKP equation,* Math. Comput. Simul. **208** (2023) 57–70.

[11] W.X. Ma, Y. Huang, F. Wang, *Inverse scattering transforms and soliton solutions of nonlocal reverse-space nonlinear Schrödinger hierarchies,* Stud. Appl. Math. **145** (2020) 563–585.

[12] M. Madadi, E. Asadi, B. Ghanbari, *Resonant Y-Type solutions, N-Lump waves, and hybrid solutions to a Ma-type model: a study of lump wave trajectories in superposition,* Phys. Scr. **98** (2023) 12–36.

[13] S. Mahmood, H. Ur-Rehman, *Existence and propagation characteristics of ion-acoustic Kadomtsev–Petviashvili (KP) solitons in nonthermal multi-ion plasmas with kappa distributed electrons,* Chaos Solitons Fractals. **169** (2023) 1–13.

[14] Y. Ohta, Yasuhiro, J. Yang, *General high-order rogue waves and their dynamics in the nonlinear Schrödinger equation,* Proc. R. Soc. Lond. Ser. A Math. Phys. Eng. Sci. **468** (2012) 1716–1740.

[15] Z. Qi, Q. Chen, M. Wang, B. Li, *New mixed solutions generated by velocity resonance in the (2+ 1)-dimensional Sawada–Kotera equation,* Nonlinear Dynam. **108** (2022) 1617–1626.

[16] S. Wang, *Novel soliton solutions of CNLSEs with Hirota bilinear method*, J. Opt. **54** (2023) 1–6.

[17] A.M. Wazwaz, *Breather wave solutions for an integrable (3+ 1)-dimensional combined pKP–BKP equation,* Chaos Solitons Fractals. **182** (2024) 1–14.

[18] X.H. Wu, Y.T. Gao, *Generalized Darboux transformation and solitons for the Ablowitz–Ladik equation in an electrical lattice,* Appl. Math. Lett. **137** (2023) 108–122.

[19] K.J. Wang, *Dynamics of complexiton, Y-type soliton and interaction solutions to the (3+1)-dimensional Kudryashov-Sinelshchikov equation in liquid with gas bubbles,* Nonlinear Dynam. **54** (2023) 1–9.

[20] Z. Zhang, X. Yang, W. Li, B. Li, *Trajectory equation of a lump before and after collision with line, lump, and breather waves for (2+ 1)-dimensional Kadomtsev–Petviashvili equation,* Chin. Phys. B. **28**, (2019), 1–18.